

Effect of shear zone on dynamic behaviour of rock tunnel constructed in highly weathered granite

Mohammad Zaid^{1a}, Md. Rehan Sadique^{*1}, M. Masroor Alam^{1b} and Manojit Samanta^{2c}

¹Department of Civil Engineering, Zakir Husain College of Engineering and Technology,
Aligarh Muslim University, Aligarh, Uttar Pradesh 202002, India

²CSIR-Central Building Research Institute, Roorkee-247667, Uttarakhand, India

(Received July 23, 2020, Revised October 7, 2020, Accepted October 16, 2017)

Abstract. Tunnels have become an indispensable part of metro cities. Blast resistance design of tunnel has attracted the attention of researchers due to numerous implosion event. Present paper deals with the non-linear finite element analysis of rock tunnel having shear zone subjected to internal blast loading. Abaqus Explicit schemes in finite element has been used for the simulation of internal blast event. Structural discontinuity i.e., shear zone has been assumed passing the tunnel cross-section in the vertical direction and consist of Highly Weathered Granite medium surrounding the tunnel. Mohr-Coulomb constitutive material model has been considered for modelling the Highly Weathered Granite and the shear zone material. Concrete Damage Plasticity (CDP), Johnson-Cook (J-C), Jones-Wilkins-Lee (JWL) equation of state models are used for concrete, steel reinforcement and Trinitrotoluene (TNT) simulation respectively. The Coupled-Eulerian-Lagrangian (CEL) method of modelling for TNT explosive and air inside the tunnel has been adopted in this study. The CEL method incorporates the large deformations for which the traditional finite element analysis cannot be used. Shear zone orientations of 0°, 15°, 30°, 45°, 60°, 75° and 90°, with respect to the tunnel axis are considered to see their effect. It has been concluded that 60° orientation of shear zone presents the most critical situation.

Keywords: rock; tunnel; blast; abaqus; finite element method; coupled Eulerian Lagrangian; Jones Wilkins Lee-equation of state; granite

1. Introduction

Tunnels serve as an important transportation medium since times immemorial. It has become a necessity in modern day metros and mega cities, as a mean of mass transit (Kenneth 2019). Hence, proper planning and designing of the tunnels plays an important role in the evolution of smart and sustainable cities. Moreover, now-a-days tunnels have become an integral part of defense and strategic storage system of a country (Daphné 2017). Their stability in general and against the extreme of intentional or accidental blast, in particular, has been a matter of concern. The use of explosive in these events is one of the common connecting part. Several researchers had studied the stability of different types of structures under blast load (Ambrosini and Luccioni 2009, Park and Krauthammer 2009, Li *et al.* 2009, Hadianfard *et al.* 2012, Sohn *et al.* 2014, Kim *et al.* 2018, Liao and Ma 2018, Lotfi and Zahrai

2018, Ewing *et al.* 2009, Ma *et al.* 2009, Guzas and Earls 2010, Mazek 2014, Abdollahzadeh and Faghihmaleki 2017, Ozacar 2018, Chen *et al.* 2019, Uyar and Aksoy 2019, Kim and Park 2019).

The performance of surrounding rockmass containing tunnel, depends upon its strength, number of joint sets, their orientation and additional presence of shear zones. The discontinuities in form of joints are ubiquitous; hence a rock mass without them cannot be envisaged. The shear zones are next to them, much less in terms of numbers, but damaging much larger area in a single go. The Granites have very commonly contains shear zones. The high number of shear zones and their varied orientations further add to the weakness of the system. As rocks may be highly strained and weak along them and need to be incorporated during tunnel design (Singh and Goel 1999).

Salang Tunnel in Afghanistan had experienced an event of internal blast in 1982. It had resulted in 1000 - 3000 deaths (Bangash and Bangash 2005). The London attack in 2005 had resulted in 52 deaths and several of injuries (Hoffman and Reinares 2014). Similar events had occurred later in 2010 – Moscow attack, in 2011 – Minsk attack, in 2015 – Bayrampasa and in 2017– Saints Petersburg etc. (Chaudhary *et al.* 2019). All these implosion events were due to use of explosives.

In case of underground tunnels, the properties of soil/rock surrounding the tunnel, amount of explosives and thickness of tunnel lining material have significant effect on the stability of tunnels (Chakraborty *et al.* 2014). Evaluation

*Corresponding author, Assistant Professor, Ph.D.

E-mail: rehan.sadique@gmail.com

^aPG Scholar, M.Tech

E-mail: mohammadzaid1@zhcet.ac.in

^bProfessor, Ph.D.

E-mail: masroor8497@rediffmail.com

^cSenior Scientist, M.Tech

E-mail: manojit@cbri.res.in

of stability of underground structures through experimental methods are not economical and involve critical safety and social issues. Therefore, advanced numerical tools offer alternate option to study the stability of underground tunnels subjected to blast loading.

Several researchers have investigated the safety and stability of underground structures (Naqvi *et al.* 2020, Zaid *et al.* 2020), in addition when subjected to blast loading (Joachim and Lundermann 1994, Ma *et al.* 1998, Wu *et al.* 1998, Chillè *et al.* 1998, Wu *et al.* 2004, Lu *et al.* 2005, Choi *et al.* 2006, Dvorak and Suvorov 2006, Gui and Chien 2006, Feldgun *et al.* 2008, Liu, 2009, Yang *et al.* 2010, Liu 2011, Zaid and Sadique, 2020a, b). Joachim and Lundermann (1994) carried out a parametric study to understand the effect of blast wave propagation inside an underground storage facility. Different parameters considered are diameter and length of the tunnel and loading density of chamber. It has been observed that the volume of underground storage and distance between the blast event and structures is the main governing criteria of stability of a structure. Higgins *et al.* (2012) investigated stability of tunnel subjected to blast loading through plane strain analysis. They incorporated the elastoplastic behavior of surrounding geomaterials though neglected the plastic behavior of concrete lining of tunnel. Kumar *et al.* (2014) studied the blast loading effect in tunnel surrounding soil medium from different sites and proposed an empirical model for assessing blast induced vibrations. The proposed empirical model is a function of the unit weight, Young's modulus and saturation density of the soil medium surrounding the tunnel. Han *et al.* (2016b) used an existing Federal Highway Administration's (FHWA) soil model to understand the interaction between the tunnel and surrounding soil under blast loading. Ability of FHWA model to incorporate the effect of excess pore-water pressure is an advantage of this model. It has been observed that an extra protective layer inside the lining of tunnel may advantageous to reduce the extent of damage due to blast loading (Gui and Chien 2006).

Wu *et al.* (1998) carried out investigation to understand the propagation behavior of blast waves in jointed rockmass. They concluded that the characteristics of joint in rock has significant effect on the pattern of blast wave propagation. Moreover, the attenuation of shock waves found to be a function of distance of propagation length, weight of charge and angle of incidence of blast waves with joint orientation. Jeon *et al.* (2015) carried out the investigation to understand the characteristics of rock fragmentation due to blasting using AUTODYN. They concluded that low quality rocks have larger diameter of crater due to blast load, therefore response of rockmass under blast loading is highly dependent on the inherent strength properties of the rockmass. Jain and Chakraborty (2018) had analyzed the performance of basalt fiber reinforced concrete lining for the tunnel through numerically. Abaqus has been used to simulate blast loading amounting 10 and 50 kg TNT explosive. The basalt fiber reinforced concrete performance has been compared with plain concrete and steel fiber reinforced concrete. It has observed that the 65% basalt fibre and 35% fiber reinforced

concrete were found to be safer than plain concrete. Xu *et al.* (2015) studied the damage and crack formation to understand the susceptibility of failure of rock tunnel subjected to internal blasting. They identified three different failure zones that are significant to cracking and contribute to failure of tunnel. They used material-point method and stress wave in the form of pressure pulse for the simulation of blast loading. Lee *et al.* (2016) and Verma *et al.* (2018) investigated the vibrations induced by blast loading in rock. The blast induced effect has been studied by the researchers and scientists through different methods and tools (Lu *et al.* 2005, Choi *et al.* 2006, Gui and Chien 2006, Feldgun *et al.* 2008a, Feldgun *et al.* 2008b, Karinski *et al.* 2009, Liu 2009, 2011, Yang *et al.* 2010, Han *et al.* 2016a, Rizvi *et al.* 2018). Song *et al.* (2018) had proposed a static force equivalence method for shear wave propagation to understand the effect of blasting on vibrations in rock tunnel. Han and Liu (2016) studies the response of a circular tunnel in saturated soil medium subjected to internal blast loading using LS-DYNA.

It has been found that the studies on the response of rock tunnel subjected to internal blast loading is still limited, especially with reference to shear zone and likewise other structural discontinuities in surrounding medium of tunnel. As the numerical tools and finite element based studies are available for the blast loading, such studies can be taken. However, the Coupled-Eulerian-Lagrangian method of modelling the TNT blast loading and air inside the tunnel has also not been considered in literature surveyed. Therefore, we have taken up the non-linear finite element analysis for the internal blast study using Coupled-Eulerian-Lagrangian modeling technique and simulation. The Abaqus/Explicit code has been utilized for the finite element analysis. Moreover, the effect of shear zone orientation has been considered and discussed in the present paper.

2. Finite element modelling

In this study, finite element based numerical technique has been employed to understand behavioral response of a rock tunnel, with shear zones, passing through, apart from the joints, under blast load from inside. The finite element software Abaqus has been adopted for the present analysis (Hibbitt *et al.* 2014, Abaqus Documentation 2014). The blast results are validated with experimental tests results from literature and found to be in a good match.

Based on the boundary convergence study, the model of rockmass surrounding the tunnel, having 30 m x 30 m in span cross-section and 35 m in length has been adopted. The tunnel opening is of 5.0 m of diameter, after the concrete liner of 0.35 m of thickness, traversed by shear zones of 2m width, passing through the tunnel transversely, having different orientations. Fig. 1 shows the geometry of different parts of the present numerical model. The different cases of shear zone orientation, at 0°, 15°, 30°, 45°, 60°, 75° and 90° with tunnel cross section are investigated in the present study, to find the most critical ones.

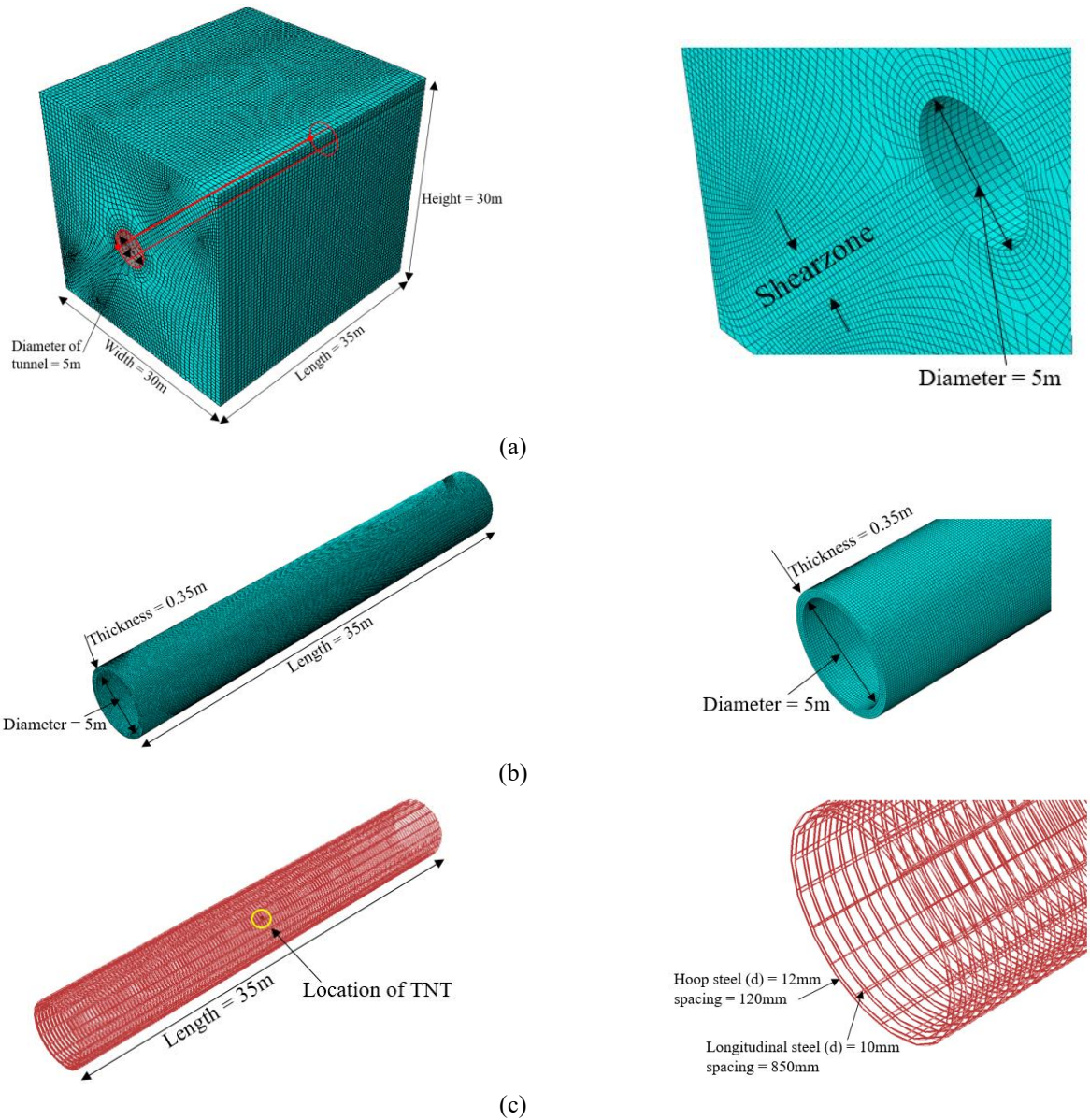


Fig. 1 Geometry of different parts of present finite element model (a) Rockmass, (b) Tunnel lining and (c) Steel reinforcement

The tunnel liner has been assumed as the doubly reinforced concrete having reinforcement in longitudinal and hoop direction. The steel bars in the longitudinal direction have 10 mm diameter, spaced at a 0.85 m from center to center. The hoop reinforcement is of 12 mm diameter bars, placed at 0.12 m of spacing from center to center in the longitudinal direction. The two rings of the hoop reinforcement have spacing at 0.25 m between them (Design Specification DMRC 2015).

Present finite element analysis considers the non-linear behavior of rock and shear zone. Therefore, the non-linear constitutive material model Mohr-Coulomb has been used. The Highly Weathered Granite has been considered as the surrounding rockmass of the tunnel with properties given in Table 1 (Gupta 1997). The nonlinear material model based on Mohr-Coulomb model, can be represented as

$$\tau = c + \sigma \tan \phi \quad (1)$$

Table 1 Mohr-Coulomb material model properties of highly weathered Granite and shear zone (Gupta 1997, Jia *et al.* 2020)

Property	Highly Weathered Granite	Shear zone
Mass Density (kg/m ³)	1970	1200
Young's Modulus (GPa)	0.3600	0.03
Poisson's Ratio	0.25	0.13
Friction Angle (°)	44.30	18.00
Cohesion (MPa)	1.36	0.30

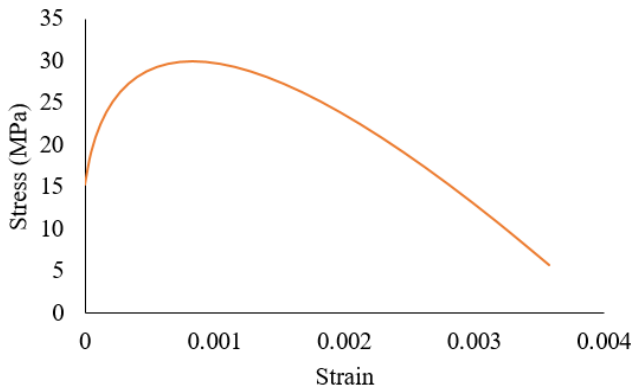
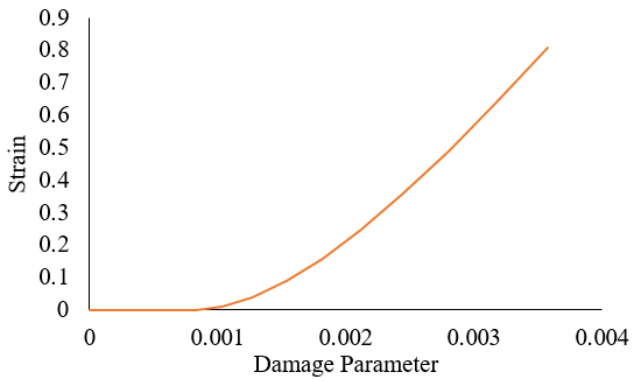
The shear stress has been represented as τ , cohesion as c , the normal stress as σ and internal friction angle as ϕ .

Moreover, the shear zone has also been modelled as the Mohr-Coulomb material. The input properties used in the present analysis for the shear zone and Highly Weathered Granite have been mentioned in Table 1.

The tunnel concrete liner has been modelled as the M30 grade concrete. Concrete Damage Plasticity (CDP) model

Table 2 Input properties of M30 grade of concrete (Hafezolghorani *et al.* 2015)

Parameter	Value
Mass Density (kg/m ³)	2500
Young's Modulus (GPa)	26.6
Poisson's Ratio	0.2
Dilation Angle (°)	31
Eccentricity	0.1
fb0/fc0	1.16
k	0.67
Viscosity Parameter	0

Fig. 2 Stress-Strain behavior of concrete in compression of M30 grade concrete (Hafezolghorani *et al.* 2015)Fig. 3 Damage behavior of concrete in compression of M30 grade concrete (Hafezolghorani *et al.* 2015)Table 3 Tensile behavior of M30 grade concrete (Hafezolghorani *et al.* 2015)

Tensile Behavior	
Stress (MPa)	Strain
2.00	0
0.02	0.000943396
Tensile Damage	
Damage	Strain
0.00	0
0.99	0.000943396

has been adopted for the modelling of non-linear behavior

of the concrete. The properties of the M30 grade of concrete are shown in Tables 2 and 3 and Figs. 2 and 3 (Hafezolghorani *et al.* 2015). Moreover, the Concrete Damage Plasticity model is represented as

$$\sigma_t = (1 - d_t)D_0^{e1}:(\varepsilon - \varepsilon_t^{e1}) \quad (2)$$

$$\sigma_c = (1 - d_c)D_0^{e1}:(\varepsilon - \varepsilon_c^{e1}) \quad (3)$$

where, t represents the tension and c represents the compression behavior of concrete, σ_t is the tensile stress vector and σ_c is the compressive stress vector, ε_t^{e1} is the plastic strains in tension and ε_c^{e1} is the plastic strain in compression, d_t is the damage variable in tension and d_c is the compression damage variable, which are considered as the function of plastic strain, and the undamaged initial elastic modulus is represented as D_0^{e1} .

The yield function in the concrete damaged plasticity model has been represented as (Lubliner *et al.* 1989, Lee and Fenves 1998)

$$F = \left(\sqrt{\frac{3}{2}} \sqrt{\bar{s} : \bar{s}} \right) - 3\alpha\bar{p} + \beta\langle \hat{\sigma}_{max} \rangle - \gamma\langle \hat{\sigma}_{max} \rangle - (1 - \alpha)\bar{\sigma}_c = 0 \quad (4)$$

wherein,

$$\alpha = \frac{\left(\frac{\sigma_{b0}}{\sigma_{c0}} \right) - 1}{2 \left(\frac{\sigma_{b0}}{\sigma_{c0}} \right) - 1} \quad (5)$$

$$\beta = \frac{\bar{\sigma}_c}{\bar{\sigma}_t} (1 - \alpha) - (1 + \alpha) \quad (6)$$

$$\gamma = \frac{3(1 - K_c)}{2K_c - 1} \quad (7)$$

$$\bar{\sigma}_c = \frac{\sigma_c}{(1 - d_t)} \quad (8)$$

$$\bar{\sigma}_t = \frac{\sigma_t}{(1 - d_t)} \quad (9)$$

where, the maximum principal effective stress has been denoted as $\hat{\sigma}_{max}$, deviatoric stress tensor as \bar{s} ,

$$\frac{\sigma_{b0}}{\sigma_{c0}} = \frac{\text{initial equibiaxial compressive yield stress}}{\text{initial uniaxial compressive yield stress}}$$

d_t has been used to represent damage variable, and

$$K_c = \frac{\text{second deviatoric stress invariant on the tensile meridian}}{\text{compressive meridian at initial crushing}}, \quad p = \frac{\sigma_1 + \sigma_2 + \sigma_3}{3}$$

The steel bars have been used as the reinforcement for tunnel lining and the Johnson-Cook material model has been considered as its constitutive material model. The properties of steel have been mentioned in the Table 4 and Fig. 4 (IS 456 2000). The Johnson-Cook model of the materials has been defined as:

$$\sigma^o = (A + B(\varepsilon^p)^n)(1 + C \ln(\frac{\dot{\varepsilon}^p}{\dot{\varepsilon}_0}))(1 - \hat{T}^m) \quad (10)$$

σ^o = the yield strength of steel,

ε^p = the effective plastic strain,

ε_0 and C are material parameters measured at or below transition temperature and A, B, C are the material constants.

Table 5 shows the properties of the Trinitrotoluene (TNT) explosive. In the present study, the TNT has been modelled as Jones-Wilkins-Lee material model based on Equation-of-State (EOS). The pressure, p is calculated for the TNT explosive by Jones-Wilkins-Lee (JWL) model for the equation of state (EOS) as given by Larcher and Casadei (2010) is

$$p = A \left(1 - \frac{\omega}{R_1 \bar{\rho}}\right) e^{-R_1 \bar{\rho}} + B \left(1 - \frac{\omega}{R_2 \bar{\rho}}\right) e^{-R_2 \bar{\rho}} + \omega \rho e_{int} \quad (11)$$

Table 4 Input properties of steel reinforcement (IS 456, 2000)

Parameter	Value
Mass Density (kg/m ³)	7800
Young's Modulus (GPa)	210
Poisson's Ratio	0.3
A (MPa)	375
B (MPa)	600
n	0.07
C	0.09
Strain Rate (s ⁻¹)	50

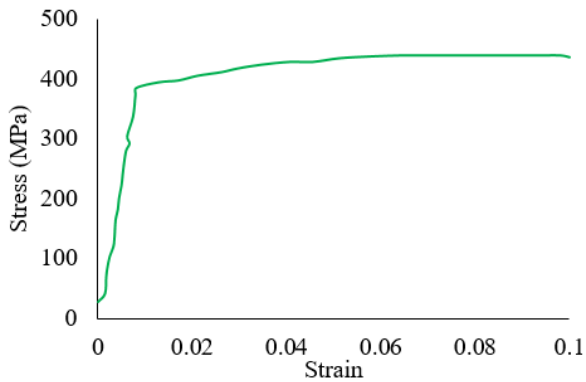


Fig. 4 Stress strain behavior of Fe415 grade of steel (IS 456 2000)

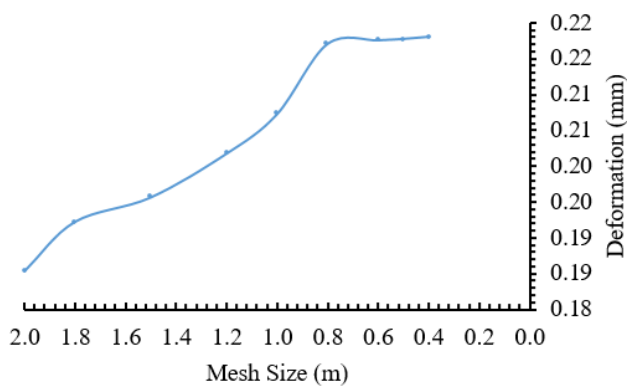


Fig. 5 Mesh convergence study

Table 5 Input properties of TNT explosive for JWL-EOS model (Larcher and Casadei 2010)

Parameter	Value
Mass Density (kg/m ³)	1630
Detonation Wave Speed (m/s)	6930
A (GPa)	373.8
B (GPa)	3.747
ω	0.35
R ₁	4.15
R ₂	0.9
Detonation Energy Density (kJ/kg)	3680

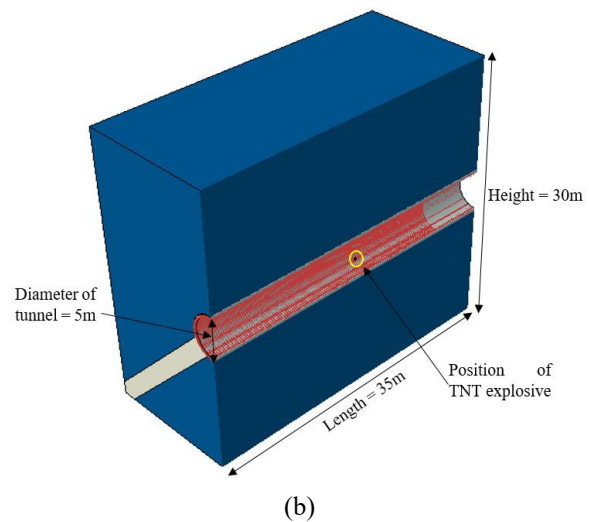
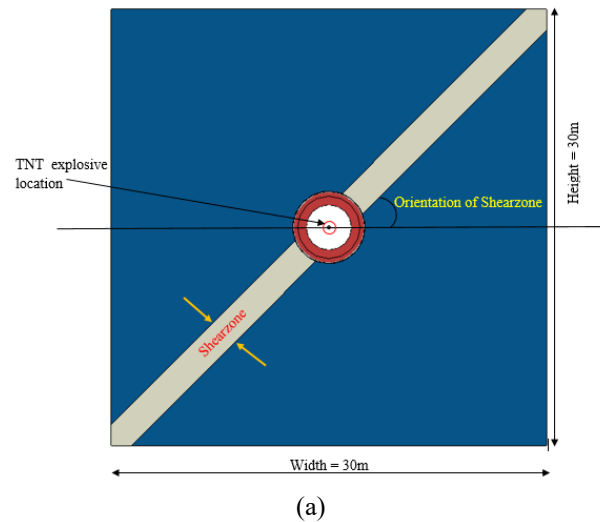


Fig. 6 Location of TNT explosive charge and shear zone (a) Front view and (b) Sectional view of the model

where, A, B, R₁, R₂ and x are material constants for TNT explosive, A and B are the pressure magnitudes, $\bar{\rho}$ is the ratio of the density ($= \frac{\rho_{sol}}{\rho}$) of the explosive, specific internal energy is represented as e_{int} at atmospheric pressure.

The first term in the above equation represent high-pressure term and second term represents low-pressure term

for the pressure observed during the explosion of charge.

In order to simulate the field conditions for the rock tunnel, the base of the model has been fixed in all directions assuming the rockmass has infinite depth. Further, the sides of the tunnel have roller support, which allows deformation in the vertical direction and restrained in other directions. The hardness and friction between the different parts of the model were simulated in the analysis by applying hard contact option in the interaction property module. Moreover, the friction has been applied by default which applies to the model by self-interaction.

C3D8R type of element available in Abaqus library has been used for rockmass meshing. C3D8R is defined as an eight-noded brick element having reduced integration allowed with hourglass control and with finite membrane strains. C3D8R element type has also been used for the concrete liner for meshing. Moreover, the steel reinforcement bars were meshed by B31 type of element, a two-node beam element. The embedment constraint has been used to ensure the proper bonding between the steel bars and the concrete lining. Fig. 5, shows the plot for the variation of deformation for different sizes of mesh. The deformations were noted at the middle length of the tunnel on the crown just above the location of the TNT explosion event. Based on mesh convergence study is has been concluded that 0.8 m size of mesh is the most optimal size for the rockmass.

The TNT explosive has been modelled using Eulerian-modelling technique. Fig. 6, shows the illustrative location of TNT explosive used in the present simulation. One of the added advantage of the Eulerian material is that it can flow through the Lagrangian mesh. Therefore, large amount of stress and deformations can be simulated by using this technique. The air inside the tunnel and the TNT explosive material has been modelled using eight node three-dimensional Continuum Eulerian with reduced integration element (EC3D8R) type. For Rockmass three dimensional 8-noded brick elements were necessary to observe the stresses and damage induced in the model. Further, as the reinforcement has been modelled as one dimensional truss element, B31 was most suited for it. EC3D8R is a Eulerian element can be used only in explicit dynamic analyses and it can contain multiple materials simultaneously. Eulerian Volume Friction (EVF) tool is available in Abaqus, which has been used for the Coupled-Eulerian-Lagrangian (CEL) modelling. EVF tool has been used for filling the Eulerian elements, as completely filled and/or partially filled by the chosen material. The material filled in Eulerian element can be tracked by EVF option. In EVF, 0 stands for completely empty elements and 1 represents Eulerian element completely filled material. In the present case, the TNT part of the model has been given $EVF = 1$, which shows that Eulerian part is completely filled by the TNT explosive charge material and it has zero percent voids. The air inside the tunnel around the TNT explosive has been modelled with $EVF = 0.8$, i.e., 20% voids. The 100 kg TNT explosive has been assumed to in the present study of internal blast loading, which is placed at the center of the tunnel, having 2.5 m distance (radius) from the internal surface of the tunnel.

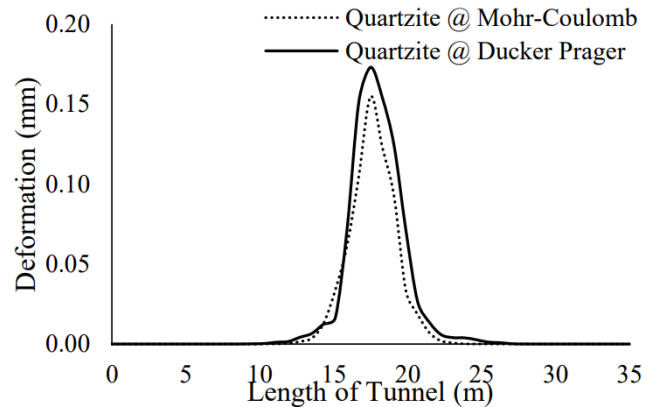


Fig. 7 Deformation profile of Quartzite tunnel under 100 kg of blast loading for comparison of strain rate effect

3. Effect of strain rate in the present case of FEM

For the validation of Mohr-Coulomb model adopted in the present paper, two analysis have compared for Quartzite rock with Mohr-Coulomb model (Gupta 1997) and Ducker Prager model (Yadav 2005). The results in both the cases show a quite similarity, therefore, the presently considered Granite rock has been validated to be used in blast loading analysis as shown in Fig. 7.

4. Validation of blast analysis

The present numerical modelling of the blast loading has been validated by comparing the experimental and numerical results from Zhao and Chen (2013). They have used LS-DYNA for the validation of experimental results and we have used Abaqus. The results are compared in Fig. 8. The two-way singly reinforced concrete slab has 1 m by 1 m of plan and 0.4 m of thickness. It has been reinforced with 6 mm bars with 75 mm spacing center to center. The properties of the steel, concrete and TNT explosive remains the same in both the studies. For concrete, Young's modulus = 28.3 GPa, Tensile strength = 4.2 MPa and Compressive strength = 39.5 MPa has been taken. While for steel, Young's modulus = 200 GPa and Yield strength = 600 MPa are taken.

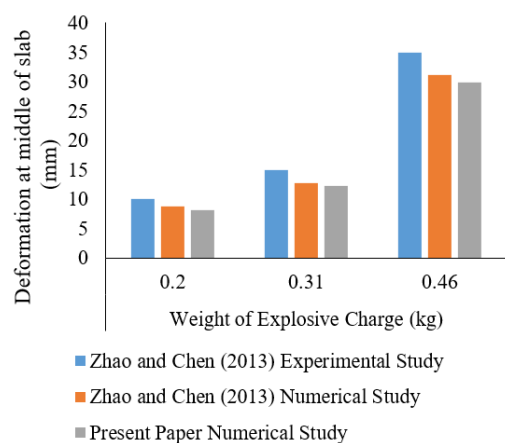


Fig. 8 Validation of deformation at the center of the slab

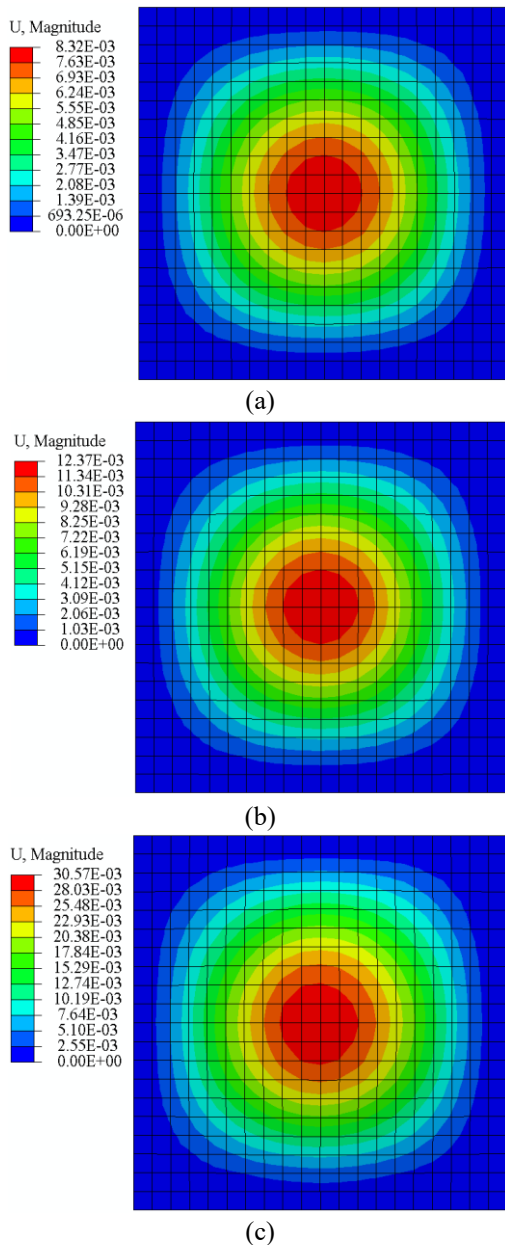


Fig. 9 Displacement contours for validation of numerical model for (a) 0.2 kg, (b) 0.31 kg and (c) 0.46 kg explosive (compared as shown by Zhao and Chen (2013))

Moreover, the geometry and boundary conditions are also similar. Three different TNT explosive charges i.e., 0.20 kg, 0.31 kg and 0.46 kg with scaled distance of $0.684 \text{ m/kg}^{1/3}$, $0.591 \text{ m/kg}^{1/3}$, and $0.518 \text{ m/kg}^{1/3}$, respectively are considered for validation. The CEL method of modelling has been considered for simulation of TNT and air materials. The properties of the TNT are similar as mentioned in previous section. For validation of numerical model for percentage, error calculated with respect to numerical results reported by Zhao and Chen (2013) is 7.4%, 3.5% and 3.8% when subjected to 0.2 kg, 0.31 kg and 0.46 kg explosive, respectively, with scaled distance of $0.684 \text{ m/kg}^{1/3}$, $0.591 \text{ m/kg}^{1/3}$, and $0.518 \text{ m/kg}^{1/3}$, respectively. In addition, experimental results are compared

with the present numerical results for validation, and 18.5%, 18.3% and 14.5% of error has been observed when subjected to 0.2 kg, 0.31 kg and 0.46 kg explosive, respectively, with scaled distance of $0.684 \text{ m/kg}^{1/3}$, $0.591 \text{ m/kg}^{1/3}$, and $0.518 \text{ m/kg}^{1/3}$, respectively. The deformation contours of RCC slab are presented in Fig. 9. Therefore, the close matching of results of present analysis proves the effective modelling techniques adopted in the present study.

5. Results and discussion

The shear zone of 2 m width passing through the section of the tunnel and along its length in the Highly Weathered Granite. The present finite element analysis has been carried out by following a flowchart, presented in Fig. 10.

Fig. 11 shows the contours of deformation obtained in different cases of shear zone orientations. The maximum deformation obtained for 0° , 15° , 30° , 45° , 60° , 75° and 90° orientation of Shear zone is 107.24 mm, 107.33 mm, 124.96 mm, 130.50 mm, 134.28 mm, 112.07 mm and 105.98 mm respectively. Hence, in a tunnel the orientation of shear zone in perfectly horizontal and vertical condition have been found to be relative safer than oblique. Especially, when it is oriented 60° to the horizontal axis. It is the most critical orientation of Shear zone in Highly Weathered Granite rock. Since, the tunnel considered is a lined one, thus, for 90° orientations the complete weight of Shear zone has been taken up by RC lining of tunnel and minimum deformation are observed for it. Moreover, overburden load has been distributed through arch action of RC lining to strata underneath.

When a geo-material deforms, the energy is stored in form of strain energy. Therefore, strain energy is an

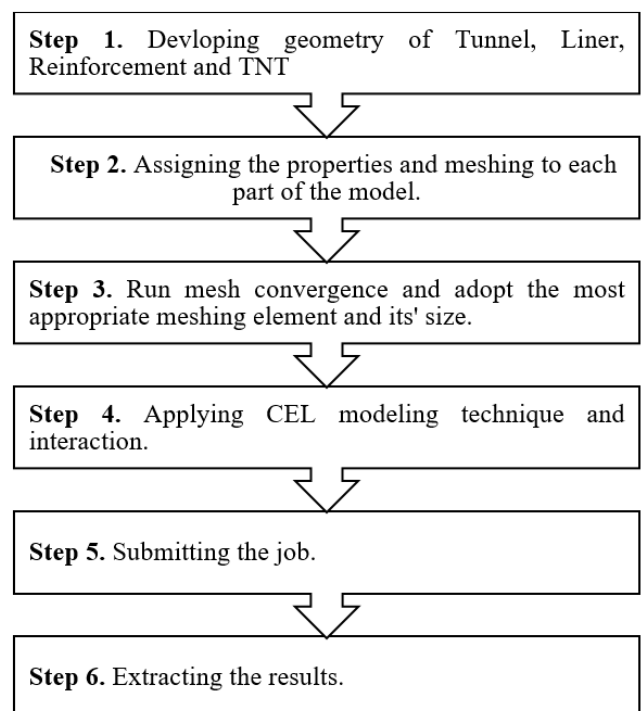


Fig. 10 Flowchart of FEM technique for blast loading

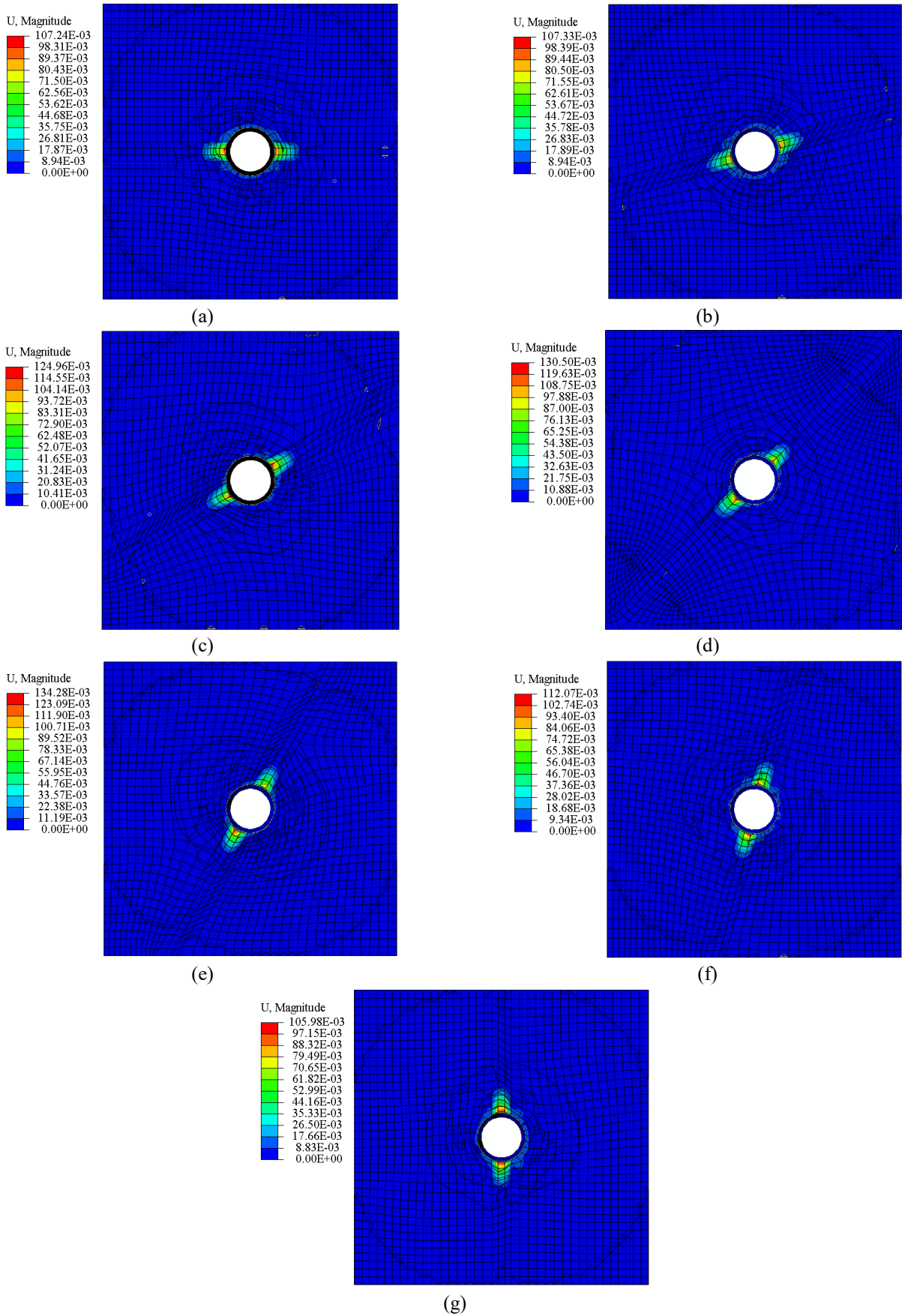


Fig. 11 Deformation contours of highly weathered Granite having different orientation (a) 0°, (b) 15°, (c) 30°, (d) 45°, (e) 60°, (f) 75° and (g) 90° of Shear zone

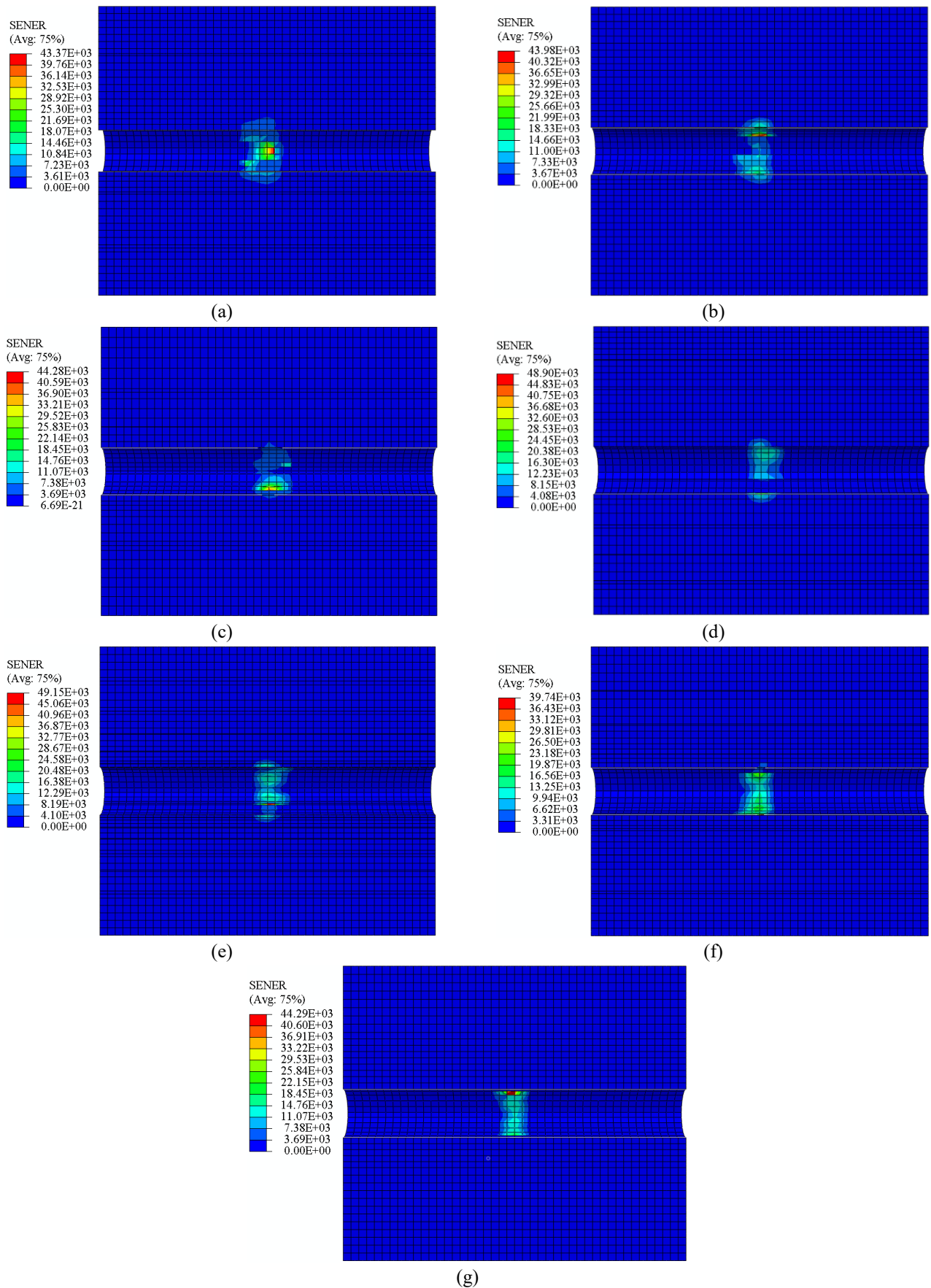


Fig. 12 Contours of strain energy for different orientation of Shear zone in highly weathered Granite rock, (a) 0°, (b) 15°, (c) 30°, (d) 45°, (e) 60°, (f) 75° and (g) 90° orientation

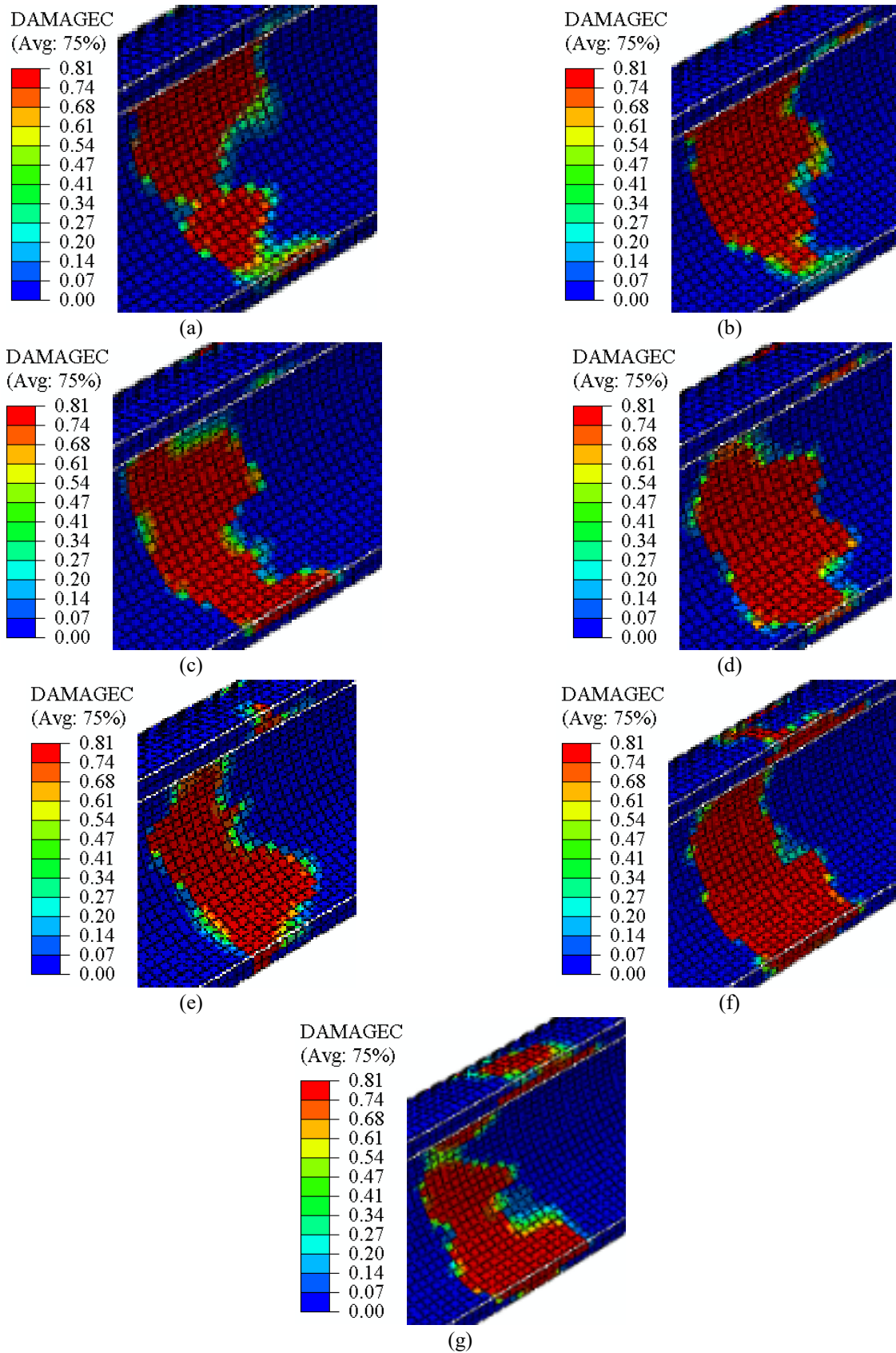


Fig. 13 Contours of compression damage in tunnel lining for different orientation of shear zone, (a) 0°, (b) 15°, (c) 30°, (d) 45°, (e) 60°, (f) 75° and (g) 90° orientation

important parameter to observe the deformation or displacement in a rock tunnel. Color contours of stain

energy are shown in Fig. 12 for different orientations of shear zone for the studied rock. By comparing the different

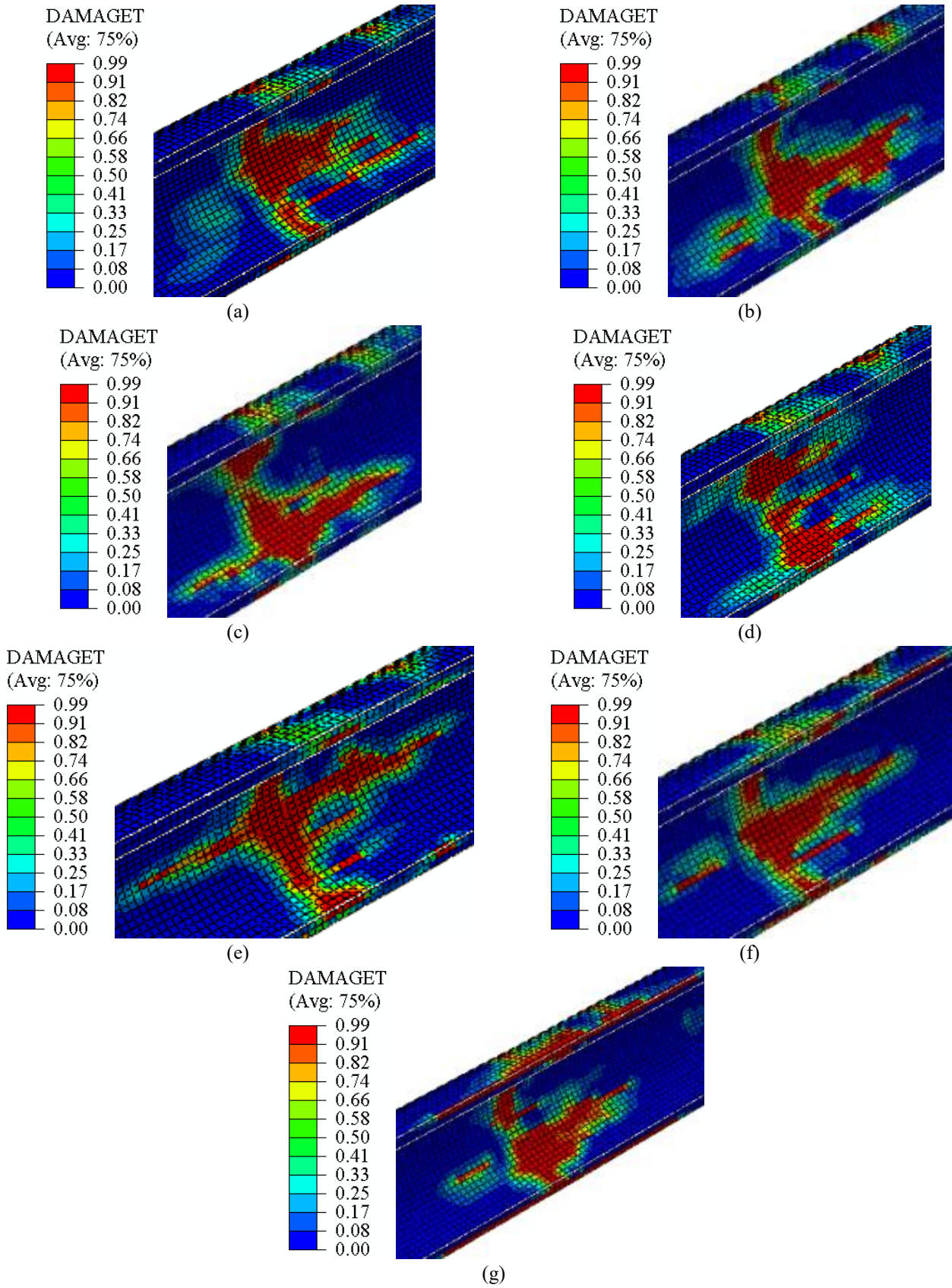


Fig. 14 Contours of tension damage in tunnel lining for different orientation of shear zone, (a) 0°, (b) 15°, (c) 30°, (d) 45°, (e) 60°, (f) 75° and (g) 90° orientation

contours, it can be discerned that maximum strain energy has been stored in case of 60° orientation of Shear zone.

Additionally, the strain energy stored for 0°, 15°, 30°, 45°, 60°, 75° and 90° orientation of Shear zone is 43.37 kJ, 43.98

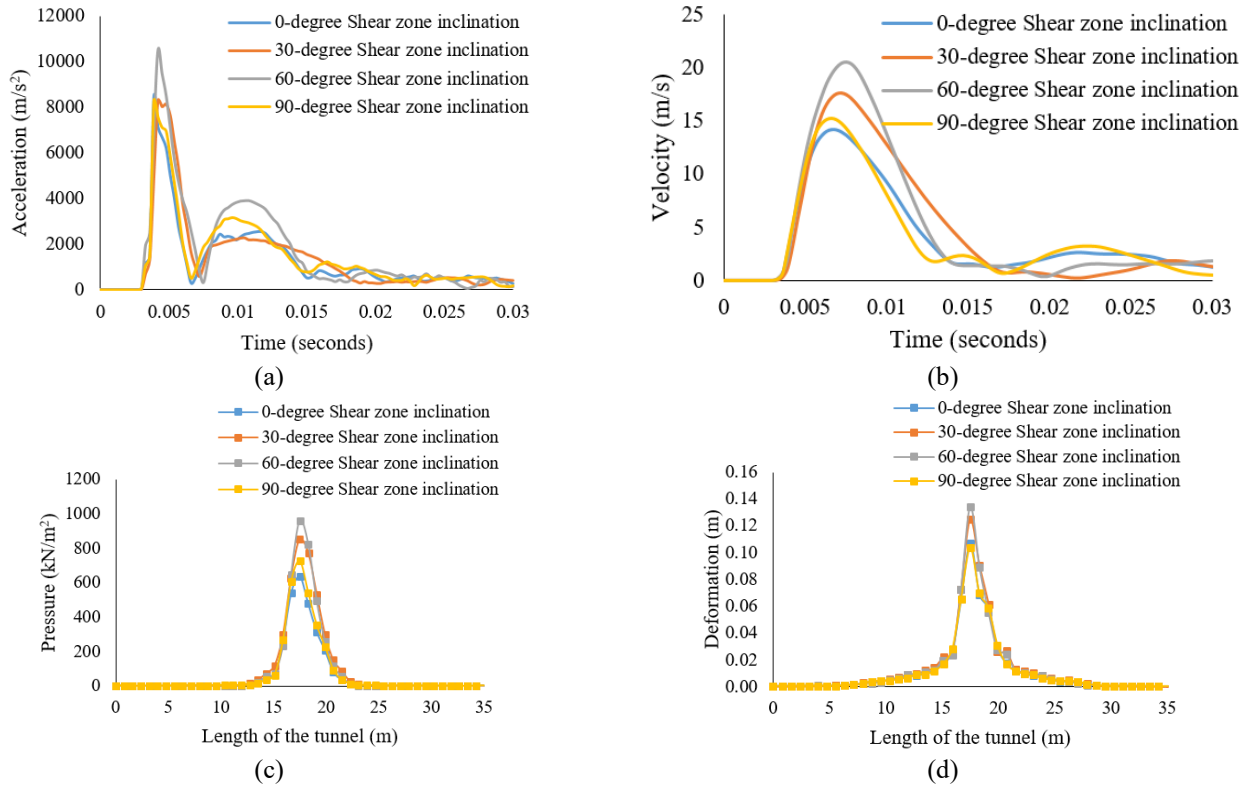


Fig. 15 (a) Acceleration vs Time response of different orientations of shear zone (At middle of the tunnel length), (b) Velocity vs Time response of different orientations of shear zone (At middle of the tunnel length), (c) Pressure vs Time response of different orientations of shear zone (At middle of the tunnel length) and (d) Deformation vs Time response of different orientations of shear zone (At middle of the tunnel length)

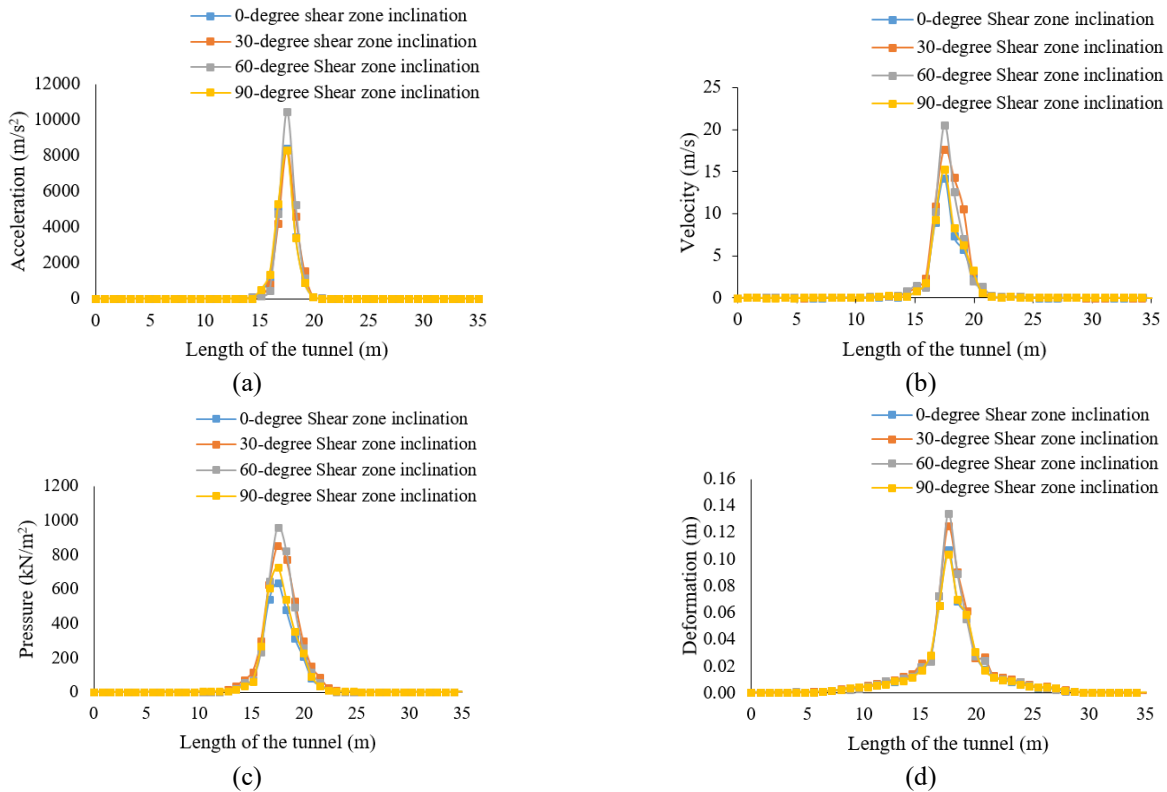


Fig. 16 (a) Acceleration profile along the longitudinal axis of the tunnel for comparison of different orientations of shear zone, (b) Velocity profile along the longitudinal axis of the tunnel for comparison of different orientations of shear zone, (c) Pressure profile along the longitudinal axis of the tunnel for comparison of different orientations of shear zone and (d) Deformation profile along the longitudinal axis of the tunnel for comparison of different orientations of shear zone

kJ, 44.28 kJ, 48.90 kJ, 49.15 kJ, 39.74 kJ and 44.29 kJ respectively. Therefore, 60° orientation of Shear zone is the most critical orientation and if such a Shear zone is present then, extra precaution must be adopted while designing the tunnel for it.

The compression damage of the RC lining for different cases has been compared in Fig. 13. From the comparison of all the contours of compression damage, it has been observed that in all the cases only internal surface of the RC lining has failed in compression except 90° orientation of shear zone. The main reason for maximum compression damage in 90° orientation of Shear zone is that the overall load of shear zone has been taken up by RC lining and due to arch action of curvature the load has been transferred by circumferential stresses.

Similarly, in Fig. 14, the tension damage of the RC lining has been compared by showing the different contour diagrams. Middle length of RC lining in all the cases has failed in tension but maximum failure has been observed for 60° orientation of Shear zone and the failure is located along springer position. Thus, 60° orientation of shear zone is also critical for tension failure in RC lining.

The variation of acceleration with time for different orientations of shear zone has been compared in Fig. 15(a) and was found that the response of acceleration is similar for all the different orientations of Shear zone. But here also, maximum acceleration has been observed for 60° orientation confirming its criticality. The variation of velocity with time has been plotted in Fig. 15(b). It can be seen that 60° orientation of shear zone is the most critical case where peak velocity has also been observed to be of late time period as compared to other cases.

The variation of pressure at the Shear zone has been shown in Fig. 15(c) for the comparison of different orientations. The pressure versus time response in all the shear zone orientation are unique for each case. The maximum crest height has been observed in 60° orientation case. The deformation versus time response for different orientations of shear zone has been compared in Fig. 15(d). As seen in previous graphs, similar response has been observed for all the different shear zone orientations. Therefore, when a tunnel design engineering came across Shear zone, which is passing the tunnel, its orientation has significant effect of the failure of overall geotechnical structure, especially the one having 60° orientation.

The acceleration is one of the most accepted output result to understand the response of a geomaterial (soil or rock) subjected to blast loading. The particle acceleration in the case of blast loading occurs when a nonlinear incident of shock waves occurs. Fig. 16(a) has been plotted for the variation of acceleration along the length of tunnel for different orientations of shear zone. In all the cases of shear zone, maximum acceleration has been concentrated only at 5 m length in the middle longitudinal direction of tunnel. The response pattern is similar in all the cases and 60° orientation of shear zone having maximum acceleration resulting it a most critical orientation. The vulnerability at this very orientation can be related to the alignment of shear zone with that of “Springer” which is an area already compromised due to high level of stress concentrations. The response of velocity along the longitudinal direction of

tunnel has been compared for different orientation of shear zone in Fig. 16(b). The 7 m length of the tunnel has the maximum disturbance and value of velocity diminishes towards the boundary of the model. The pressure response along the longitudinal direction of the tunnel has been compared for different orientations of Shear zone in Fig. 16(c). The maximum variation of pressure has been observed in the middle 11 m length of tunnel and 60° orientation of shear zone has experienced maximum pressure and maximum damage. Therefore, the location of blast event has major role in the failure patterns of different parameters. It has been observed that more than 20 m length of Highly Weathered Granite rock has been subjected to deformations, which diminishes with the distance along the length of tunnel as shown in Fig. 16(d). Although, response of all cases remains similar and 60° orientation of shear zone having maximum deformations.

6. Conclusions

Rockmass are inherently discontinuous due to presence of several geological structure. Shear zone had been found to be one of the most prominent structural discontinuity in tectonically active areas. A three dimensional finite element study has been carried out using CEL method to understand the effect of shear zone on rock tunnel subjected to internal blast. Displacement, strain energy, displacement velocity and pressure in the rockmass are evaluated. Damage in the concrete lining has been evaluated for both compressive and tensile forces generated during blast. Tunnels crossing the shear zone at 60° with the horizontal has been found to be least resistant against the blast load, in the present study. This excessive damage can be ascribed to the alignment of shear zone with that of “Springer” which is an area already compromised, due to high concentration of stresses. Overall, compression damage was dominant on the face; however, tension damage appeared dominating along the lining thickness. Therefore, tunnel has experienced significant loss of serviceability. Moreover, it has been observed that orientation of shear zone plays a significant role in the overall serviceability of tunnel when subjected to an internal blast loading. Effect of shear zone size and response in tunnel without lining is not included here and constitute future scope of work.

Acknowledgments

The first author also acknowledges the PG-GATE-201819 (ID-201819-PGGATE-10072-332) scholarship received from University Grants Commission, India, during the course of this work.

References

- Abaqus Documentation (2014), Dassault Systèmes, Providence, Rhode Island, U.S.A.
- Abdollahzadeh, G. and Faghimaleki, H. (2017), “A method to evaluate the risk-based robustness index in blast-influenced structures”, *Earthq. Struct.*, **12**(1), 47-54.

- <https://doi.org/10.12989/eas.2017.12.1.047>.
- Ambrosini, D. and Luccioni, B.M. (2009), "Reinforced concrete wall as protection against accidental explosions in the petrochemical industry", *Struct. Eng. Mech.*, **32**(2), 213-233. <https://doi.org/10.12989/sem.2009.32.2.213>.
- Bangash, M. and Bangash, T. (2005), *Explosion-Resistant Buildings: Design, Analysis, and Case Studies*, Springer-Verlag Berlin Heidelberg, Heidelberg, Germany.
- Chaudhary, R.K., Mishra, S., Chakraborty, T. and Matsagar, V. (2019), "Vulnerability analysis of tunnel linings under blast loading", *Int. J. Protect. Struct.*, **10**(1), 73-94. <https://doi.org/10.1177/2041419618789438>.
- Chen, L., Zhou, Z., Zang, C., Zeng, L. and Zhao, Y. (2019), "Failure pattern of large-scale goaf collapse and a controlled roof caving method used in gypsum mine", *Geomech. Eng.*, **18**(4), 449-457. <https://doi.org/10.12989/gae.2019.18.4.449>.
- Chillè, F., Sala, A. and Casadei, F. (1998), "Containment of blast phenomena in underground electrical power plants", *Adv. Eng. Softw.*, **29**(1), 7-12. [https://doi.org/10.1016/S0965-9978\(97\)00047-1](https://doi.org/10.1016/S0965-9978(97)00047-1).
- Choi, S., Wang, J., Munfakh, G. and Dwyre, E. (2006), "3D nonlinear blast model analysis for underground structures", *Proceedings of the GeoCongress 2006: Geotechnical Engineering in the Information Technology Age*, Atlanta, Georgia, U.S.A., February-March.
- DMRC (2015), Design specifications, DMRC, Barakhamba road, New Delhi, India.
- Dvorak, G. and Suvorov, A. (2006), "Protection of sandwich plates from low-velocity impact", *J. Compos. Mater.*, **40**(15), 1317-1331. <https://doi.org/10.1177/0021998305059053>.
- Ewing, C.M., Guillin, C., Dhakal, R.P. and Chase, J.G. (2009), "Spectral analysis of semi-actively controlled structures subjected to blast loading", *Struct. Eng. Mech.*, **33**(1), 79-93. <https://doi.org/10.12989/sem.2009.33.1.079>.
- Feldgun, V. R., Kochetkov, A.V., Karinski, Y.S. and Yankelevsky, D.Z. (2008a), "Internal blast loading in a buried lined tunnel", *Int. J. Impact Eng.*, **35**(3), 172-183. <https://doi.org/10.1016/j.ijimpeng.2007.01.001>.
- Feldgun, V., Kochetkov, A.V., Karinski, Y.S. and Yankelevsky, D.Z. (2008b), "Blast response of a lined cavity in a porous saturated soil", *Int. J. Impact Eng.*, **35**(9), 953-966. <https://doi.org/10.1016/j.ijimpeng.2007.06.010>.
- Gui, M.W. and Chien, M.C. (2006), "Blast-resistant analysis for a tunnel passing beneath Taipei Shongsan airport - A parametric study", *Geotech. Geol. Eng.*, **24**(2), 227-248. <https://doi.org/10.1007/s10706-004-5723-x>.
- Gupta, A.S. (1997), *Engineering Behavior and Classification of Weathering Rock*, Indian Institute of Technology Delhi, Delhi, India.
- Guzas, E.L. and Earls, C.J. (2010), "Air blast load generation for simulating structural response", *Steel Compos. Struct.*, **10**(5), 429-455. <https://doi.org/10.12989/scs.2010.10.5.429>.
- Hadianfard, M.A., Farahani, A. and B-Jahromi, A. (2012), "On the effect of steel columns cross sectional properties on the behaviours when subjected to blast loading", *Struct. Eng. Mech.*, **44**(4), 449-463. <https://doi.org/10.12989/sem.2012.44.4.449>.
- Hafezolzghorani, M., Hejazi, F., Vaghei, R., Jaafar, M.S.B. and Karimzade, K. (2015), "Simplified damage plasticity model for concrete", *Struct. Eng. Int.*, **27**(1), 68-78. <https://doi.org/10.2749/101686616X1081>.
- Han, Y. and Liu, H. (2016), "Failure of circular tunnel in saturated soil subjected to internal blast loading", *Geomech. Eng.*, **11**(3), 421-438. <https://doi.org/10.12989/gae.2016.11.3.421>.
- Han, Y., Zhang, L. and Yang, X. (2016a), "Soil-tunnel interaction under medium internal blast loading", *Procedia Eng.*, **143**, 403-410. <https://doi.org/10.1016/j.proeng.2016.06.051>.
- Han, Y., Zhang, L. and Yang, X. (2016b), "Soil-tunnel interaction under medium internal blast loading", *Procedia Eng.*, **143**, 403-410. <https://doi.org/10.1016/j.proeng.2016.06.051>.
- Hibbitt, D., Karlsson, B. and Sorensen, P. (2014), *ABAQUS User-Manual Release 6.14.*, Dassault Systèmes Simulia Corporation, Providence, Rhode Island, U.S.A.
- Higgins, W., Chakraborty, T. and Basu, D. (2012), "A high strain-rate constitutive model for sand and its application in finite element analysis of tunnels subjected to blast", *Int. J. Numer. Anal. Meth. Geomech.*, **37**(15), 2590-2610. <https://doi.org/10.1002/nag.2153>.
- Hoffman, B. and Reinares, F. (2014), *The Evolution of the Global Terrorist Threat: From 9/11 to Osama Bin Laden's Death*, Columbia University Press, New York, U.S.A.
- IS 456 (2000), Plain and Reinforced Concrete - Code of Practice. New Delhi, India.
- Jain, P. and Chakraborty, T. (2018), "Numerical analysis of tunnel in rock with basalt fiber reinforced concrete lining subjected to internal blast load", *Comput. Concrete*, **21**(4), 399-406. <https://doi.org/10.12989/cac.2018.21.4.399>.
- Jeon, S., Kim, T.H. and You, K.H. (2015), "Characteristics of crater formation due to explosives blasting in rock mass", *Geomech. Eng.*, **9**(3), 329-344. <https://doi.org/10.12989/gae.2015.9.3.329>.
- Jia, S., Zhao, Z., Wu, G., Wu, B. and Wen, C. (2020), "A coupled elastoplastic damage model for clayey rock and its numerical implementation and validation", *Geofluids*. <https://doi.org/10.1155/2020/9853782>.
- Joachim, C. and Lundermann, C. (1994), "Parameter study of underground ammunition storage magazines", U.S. Army Engineer Waterways Experiment Station, Vicksburg, Mississippi, U.S.A.
- Karinski, Y.S., Feldgun, V.R. and Yankelevsky, D.Z. (2009), "Explosion-induced dynamic soil-structure interaction analysis with the coupled Godunov-variational difference approach", *Int. J. Numer. Meth. Eng.*, **77**(6), 824-851. <https://doi.org/10.1002/nme.2436>.
- Kim, D. and Park, K. (2019), "Study on the characteristics of grout material using ground granulated blast furnace slag and carbon fiber", *Geomech. Eng.*, **19**(4), 361-368. <https://doi.org/10.12989/gae.2019.19.4.361>.
- Kim, S. H., Woo, H., Choi, G. and Yoon, K. (2018), "A new concept for blast hardened bulkheads with attached aluminum foam", *Struct. Eng. Mech.*, **65**(3), 243-250. <https://doi.org/10.12989/sem.2018.65.3.243>.
- Kumar, R., Choudhury, D. and Bhargava, K. (2014), "Prediction of blast-induced vibration parameters for soil sites", *Int. J. Geomech.*, **14**(3), 04014007. [https://doi.org/10.1061/\(ASCE\)GM.1943-5622.0000355](https://doi.org/10.1061/(ASCE)GM.1943-5622.0000355).
- Lane, K.S. (2019), Tunnels and underground excavations | History, Methods, Uses, & Facts, Britannica. <https://www.britannica.com/technology/tunnel>.
- Larcher, M. and Casadei, F. (2010), "Explosions in complex geometries—A comparison of several approaches", *Int. J. Protect. Struct.*, **1**(2), 169-195. <https://doi.org/10.1260/2041-4196.1.2.169>.
- Lee, J. and Fenves, G. (1998), "Plastic damage model for cyclic loading of concrete structures", *J. Eng. Mech.*, **124**(8), 892-900. [https://doi.org/10.1061/\(ASCE\)0733-9399\(1998\)124:8\(892\)](https://doi.org/10.1061/(ASCE)0733-9399(1998)124:8(892)).
- Lee, J.S., Ahn, S.K. and Sagong, M. (2016), "Attenuation of blast vibration in tunneling using a pre-cut discontinuity", *Tunn. Undergr. Sp. Technol.*, **52**, 30-37. <https://doi.org/10.1016/j.tust.2015.11.010>.
- Li, G.Q., Yang, T.C. and Chen, S.W. (2009), "Behavior and simplified analysis of steel-concrete composite beams subjected to localized blast loading", *Struct. Eng. Mech.*, **32**(2), 337-350.

- <https://doi.org/10.12989/sem.2009.32.2.337>.
- Liao, J.J. and Ma, G. (2018), "Energy absorption of the ring stiffened tubes and the application in blast wall design", *Struct. Eng. Mech.*, **66**(6), 713-727.
<https://doi.org/10.12989/sem.2018.66.6.713>.
- Liu, H. (2009), "Dynamic analysis of subway structures under blast loading", *Geotech. Geol. Eng.*, **27**(6), 699-711.
<https://doi.org/10.1007/s10706-009-9269-9>.
- Liu, H. (2011), "Damage of cast-iron subway tunnels under internal explosions", *Proceedings of the Geo-Frontiers Congress 2011*, Dallas, Texas, U.S.A., March.
- Lotfi, S. and Zahrai, S.M. (2018), "Blast behavior of steel infill panels with various thickness and stiffener arrangement", *Struct. Eng. Mech.*, **65**(5), 587-600.
<https://doi.org/10.12989/sem.2018.65.5.587>.
- Lu, Y., Wang, Z. and Chong, K. (2005), "A comparative study of buried structure in soil subjected to blast load using 2D and 3D numerical simulations", *Soil Dyn. Earthq. Eng.*, **25**(4), 275-288.
<https://doi.org/10.1016/j.soildyn.2005.02.007>.
- Lubliner, J., Oliver, J., Oller, S. and Oñate, E. (1989), "A plastic-damage model for concrete", *Int. J. Solids Struct.*, **25**(3), 299-326.
[https://doi.org/10.1016/0020-7683\(89\)90050-4](https://doi.org/10.1016/0020-7683(89)90050-4).
- Ma, G., Hao, H. and Zhou, Y.X. (1998), "Modeling of wave propagation induced by underground explosion", *Comput. Geotech.*, **22**(3-4), 283-303.
[https://doi.org/10.1016/S0266-352X\(98\)00011-1](https://doi.org/10.1016/S0266-352X(98)00011-1)
- Ma, G.W., Huang, X. and Li, J.C. (2009), "Damage assessment for buried structures against internal blast load", *Struct. Eng. Mech.*, **32**(2), 301-320.
<https://doi.org/10.12989/sem.2009.32.2.301>.
- Mazek, S.A. (2014), "Performance of sandwich structure strengthened by pyramid cover under blast effect", *Struct. Eng. Mech.*, **50**(4), 471-486.
<https://doi.org/10.12989/sem.2014.50.4.471>.
- Naqvi, M.W., Akhtar, M.F., Zaid, M. and Sadique, M.R. (2020), "Effect of superstructure on the stability of underground tunnels", *Transp. Infrastruct. Geotechnol.*, 1-20.
<https://doi.org/10.1007/s40515-020-00119-6>.
- Ozacar, V. (2018), "New methodology to prevent blasting damages for shallow tunnel", *Geomech. Eng.*, **15**(6), 1227-1236.
<https://doi.org/10.12989/gae.2018.15.6.1227>.
- Park, J.Y. and Krauthammer, T. (2009), "Inelastic two-degree-of-freedom model for roof frame under airblast loading", *Struct. Eng. Mech.*, **32**(2), 321-335.
<https://doi.org/10.12989/sem.2009.32.2.321>.
- Richemond-Barak, D. (2017), *Underground Warfare*, Oxford University Press.
- Rizvi, Z.H., Khan, M.A., Sembdner, K. and Husain, S.F. (2018), "Numerical modelling of crack wave interaction with BEM", *Materials Today Proceedings*, 28253-28261.
<https://doi.org/10.1016/j.matpr.2018.10.070>.
- Singh, B. and Goel, R.K. (1999), *Rock Mass Classification, A Practical Approach in Civil Engineering*, 1st Edition, Elsevier.
- Sohn, J.M., Kim, S.J., Seong, D.J., Kim, B.J., Ha, Y.C., Seo, J.K. and Paik, J.K. (2014), "Structural impact response characteristics of an explosion-resistant profiled blast walls in arctic conditions", *Struct. Eng. Mech.*, **51**(5), 755-771.
<https://doi.org/10.12989/sem.2014.51.5.755>.
- Song, Z.P., Li, S.H., Wang, J.B., Sun, Z.Y., Liu, J. and Chang, Y.Z. (2018), "Determination of equivalent blasting load considering millisecond delay effect", *Geomech. Eng.*, **15**(2), 745-754.
<https://doi.org/10.12989/gae.2018.15.2.745>.
- Uyar, G.H., and Aksoy, C.O. (2019), "Comparative review and interpretation of the conventional and new methods in blast vibration analyses", *Geomech. Eng.*, **18**(5), 545-554.
<https://doi.org/10.12989/gae.2019.18.5.545>.
- Verma, H. K., Samadhiya, N.K., Singh, M., Goel, R.K. and Singh, P.K. (2018), "Blast induced rock mass damage around tunnels", *Tunn. Undergr. Sp. Technol.*, **71**, 149-158.
<https://doi.org/10.1016/j.tust.2017.08.019>.
- Wu, C., Lu, Y. and Hao, H. (2004), "Numerical prediction of blast-induced stress wave from large-scale underground explosion", *Int. J. Numer. Anal. Meth. Geomech.*, **28**(1), 93-109.
<https://doi.org/10.1002/nag.328>.
- Wu, Y.K., Hao, H., Zhou, Y.X. and Chong, K. (1998), "Propagation characteristics of blast-induced shock waves in a jointed rock mass", *Soil Dyn. Earthq. Eng.*, **17**(6), 407-412.
[https://doi.org/10.1016/S0267-7261\(98\)00030-X](https://doi.org/10.1016/S0267-7261(98)00030-X).
- Xu, L., Schreyer, H. and Sulsky, D. (2015), "Blast-induced rock fracture near a tunnel", *Int. J. Numer. Anal. Meth. Geomech.*, **39**(1), 23-50. <https://doi.org/10.1002/nag.2294>.
- Yadav, H.R. (2005), "Geotechnical evaluation and analysis of Delhi metro tunnels", Ph.D. Thesis, Indian Institute of Technology Delhi, New Delhi, India.
- Yang, Y., Xie, X. and Wang, R. (2010), "Numerical simulation of dynamic response of operating metro tunnel induced by ground explosion", *J. Rock Mech. Geotech. Eng.*, **2**(4), 373-384.
<https://doi.org/10.3724/SP.J.1235.2010.00373>.
- Zaid, M. and Sadique, M.R. (2020a), "The response of rock tunnel when subjected to blast loading: Finite element analysis", *Eng. Reports*, e12293. <https://doi.org/10.1002/eng2.12293>
- Zaid, M. and Sadique, M.R. (2020b), "Blast resistant behaviour of tunnels in sedimentary rocks", *Int. J. Protect. Struct.*, 204141962095121. <https://doi.org/10.1177/2041419620951211>.
- Zaid, M., Mishra, S. and Rao, K.S. (2020), *Finite Element Analysis of Static Loading on Urban Tunnels*, in *Geotechnical Characterization and Modelling*, Springer, Singapore, 807-823.
- Zhao, C.F. and Chen, J.Y. (2013), "Damage mechanism and mode of square reinforced concrete slab subjected to blast loading", *Theor. Appl. Fract. Mech.*, **63-64**, 54-62.
<https://doi.org/10.1016/j.tafmec.2013.03.006>.